NASA TECHNICAL NOTE

NASA TN D-5478

NASA TN D-5478

APPLICATION OF HUMAN TRANSFER FUNCTIONS TO SYSTEM ANALYSIS

by James J. Adams and Maxwell W. Goode

Langley Research Center
Langley Station, Hampton, Va.

NATIONAL AERONAUTICS AND SPACE ADMINISTRATION • WASHINGTON, D. C. • OCTOBER 1969

1. Report No. NASA TN D-5478	2. Government Accession No.	3. Recipient's Catalog No.
4. Title and Subtitle APPLICATION OF HUMAN TRANSFER FUNCTIONS TO SYSTEM ANALYSIS		5. Report Date October 1969
		6. Performing Organization Code
7. Author(s) James J. Adams and Maxwell W. Goode		8. Performing Organization Report No. L-6382
		10. Work Unit No. 127-51-17-07-23
9. Performing Organization Name and Address NASA Langley Research Center Hampton, Va. 23365		11. Contract or Grant No.
		13. Type of Report and Period Covered Technical Note
12. Sponsoring Agency Name and Address National Aeronautics and Space Administration Washington, D.C. 20546		14. Sponsoring Agency Code

15. Supplementary Notes

16. Abstract

An analytical study was made of a full-scale, manually controlled, lunar-landing simulator by using analytical transfer functions for the pilot control response along with the analytical representation for the mechanisms. The results of this study showed that some of the dynamic characteristics of the simulator were in a range to influence the response of the manually controlled systems that were to be tested. Tests were made in which the dynamic response of the simulator was varied over a limited range of characteristics. The results confirmed the conclusion of the analytical study in that the change did influence the piloted response.

17. Key Words Suggested by Author(s) Human transfer functions Simulators Pilot opinion Design studies of servomechanisms	18. Distribution Statement Unclassified – Unlimited

19. Security Classif. (of this report) Unclassified	20. Security Classif. (of this page) Unclassified	21. No. of Pages 30	22. Price* $3.00

*For sale by the Clearinghouse for Federal Scientific and Technical Information
Springfield, Virginia 22151

APPLICATION OF HUMAN TRANSFER FUNCTIONS TO SYSTEM ANALYSIS

By James J. Adams and Maxwell W. Goode
Langley Research Center

SUMMARY

An analytical study was made of a full-scale, manually controlled, lunar-landing simulator by using analytical transfer functions for the pilot control response along with the analytical representation for the mechanisms. The simulator reproduced lunar gravity by supporting five-sixths of the weight of the test vehicle with an overhead cable. The cable was kept directly over the test vehicle by the automatic control of the longitudinal drive mechanism of the simulator. The results showed that some of the dynamic characteristics of the simulator were in a range to influence the response of the manually controlled systems which were to be tested.

The results of the analytical study were checked by actual operation of the simulator. The simulator was operated with the gain of the longitudinal drive set as high as was possible with the actual mechanism and with a lower gain to determine whether this change would affect the pilot's response. The pilots reported that the slower responding system (low gain) was more difficult to control. The records clearly showed a decrease in system damping with the degraded system.

INTRODUCTION

One of the reasons for determining human transfer functions is to allow evaluation and prediction of the performance of manually controlled systems during design studies. This report explains the use of such transfer functions in an analysis of the drive system of a lunar-landing simulator to determine the effect of the drive system characteristics on the performance of the pilot-vehicle combination.

The lunar-landing simulator is a manually controlled six-degree-of-freedom moving-base, lunar-gravity simulation device designed to define desirable handling qualities for a lunar-landing vehicle and piloting problems associated with lunar-landing maneuvers. Since no direct comparison could be made between the simulator and the actual cases, it was desirable to define the influence of the simulator on the piloting tasks. In this effort analytical transfer functions for pilot control responses and an analytical representation of the drive mechanisms were used.

The transfer functions used to describe the pilot's control action were derived in reference 1. These transfer functions describe the control used by the pilot when controlling a multi-loop system representative of the lunar-landing horizontal-translation maneuver. The use of these pilot transfer functions in determining the most suitable simulator drive characteristics is presented.

SYMBOLS

A_L equivalent leakage orifice area, ft^2 (m^2)

A_{RV} relief valve area, ft^2 (m^2)

a speed of propagation, ft/sec (m/sec)

B_L load viscous friction, $\frac{\text{in-lb}}{\text{rad/sec}}$ $\left(\frac{\text{m-N}}{\text{rad/sec}}\right)$

B_m motor damping, $\frac{\text{in-lb}}{\text{rad/sec}}$ $\left(\frac{\text{m-N}}{\text{rad/sec}}\right)$

D_m motor displacement, in^3 (cm^3)

D_p pump displacement, in^3 (cm^3)

d distance from whiffletree to vehicle, ft (m)

g gravity, 32.2 ft/sec^2 (9.81 m/sec^2)

h maximum deflection of first cable vibration mode, ft (m)

J_L load inertia, in-lb-sec^2 (m-N-sec^2)

J_m motor inertia, in-lb-sec^2 (m-N-sec^2)

K_L leakage coefficient, $\frac{\text{in}^3/\text{sec}}{\text{psi}}$ $\left(\frac{\text{cm}^3/\text{sec}}{\text{N/m}^2}\right)$

K_m torque coefficient, $\frac{\text{in-lb}}{\text{rad/sec}}$ $\left(\frac{\text{m-N}}{\text{rad/sec}}\right)$

K_o orifice flow coefficient, $\frac{\text{in}^2\text{-lb}^{1/2}}{\text{sec}}$ $\left(\frac{\text{m}^2\text{-N}^{1/2}}{\text{sec}}\right)$

K_t tire torsional spring constant, in-lb/rad (m-N/rad)

K_1, K_2, τ	gains in analytical transfer function of pilot
$K_\varphi, K_{\dot{\varphi}}$	simulator drive system control gains
k	constant
l	pendulum length, ft (m)
l'	whiffletree coordinate, ft (m)
m	mass, slugs (kg)
n	gear ratio
p_m	motor pressure, lb/in^2 (N/m^2)
Q_c	compressible flow, in^3/sec (cm^3/sec)
Q_L	leakage flow, in^3/sec (cm^3/sec)
Q_m	motor flow, in^3/sec (cm^3/sec)
Q_p	pump flow, in^3/sec (cm^3/sec)
Q_{RL}	relief valve flow, in^3/sec (cm^3/sec)
R	tire radius, in. (cm)
s	Laplace operator, per second
T	tension, lb (N)
T_L	tire torque, in-lb (N-m)
T_m	induction motor torque, in-lb (m-N)
t	time, sec
V	oil volume under compression, in^3 (cm^3)

w'	cable density, lb/ft (N/m)
x	translation, ft (m)
z,y	cable coordinates, ft (m)
β	bulk modulus of oil, lb/in^2 (N/m^2)
δ	control moment, rad/sec^2
θ	pitch-attitude angle, radians
τ_f	filter breakpoint frequency, rad/sec
ϕ	pendulum angle, radians
ψ_m	motor angle, rad
ψ_L	load shaft angle, rad
ω_m	motor speed, rad/sec
ω_n	undamped natural frequency, rad/sec
ω_p	pump speed, rad/sec
ω_{sync}	synchronous speed, rad/sec

Subscripts:

B	bridge
V	vehicle
c	command
e	error
f	filter
w	whiffletree
m	motor

Dots over symbols denote derivatives with respect to time.

DESCRIPTION OF PROBLEM

Simulator

The description and operation of the lunar-landing simulator are given in detail in reference 2. The simulator itself is shown in figure 1. Basically, the simulator is a six-degree-of-freedom, moving base, lunar-gravity simulator with a flight envelope 360 feet (110 m) by 42 feet (13 m) by 180 feet (55 m) high. Lunar gravity is simulated by supporting five-sixths of the weight of the test vehicle with a cable suspension system. The tension in the cables is regulated by measuring the load with a strain gage and operating an overhead winch in response to the error in the measured tension. The suspension cables are kept directly over the vehicle by measuring the angle of the cables with respect to the vertical and driving a traveling bridge in response to this measured angle. The longitudinal drive system of the traveling bridge is the subject of study in this report. See sketch (a).

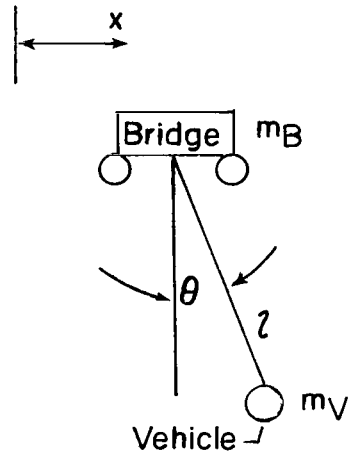

Sketch (a).- Bridge and vehicle.

Simplified equations defining the longitudinal motion of the overhead bridge and the cable-supported vehicle are:

$$\left(m_B + m_V\right)\ddot{x}_B + m_V l\ddot{\varphi} = 0 \tag{1}$$

$$m_V l\ddot{x}_B + m_V l^2\ddot{\varphi} + m_V g l\varphi = 0 \tag{2}$$

The characteristic equation for the system in Laplace notation is

$$s^2\left[\left(m_B + m_V\right)\left(m_V l^2\right)s^2 + \left(m_B + m_V\right)\left(m_V g l\right) - m_V{}^2 l^2 s^2\right] = 0 \tag{3}$$

which is the familiar equation for a pendulum in which the frequency is primarily determined by the length l but with an additional term representing the influence of the

pendulum pivot point being free to move and increasing the frequency somewhat. If bridge acceleration is a function of φ and $\dot{\varphi}$, the equations of motion become

$$\left(m_B + m_V\right)\ddot{x}_B + m_V l\ddot{\varphi} = K_\varphi \varphi + K_{\dot{\varphi}}\dot{\varphi} \tag{4}$$

$$m_V l\ddot{x}_B + m_V l^2\ddot{\varphi} + m_V g l\varphi = 0 \tag{5}$$

the characteristic equation, in Laplace notation, being:

$$s^2\left[\left(m_B + m_V\right)\left(m_V l^2\right)s^2 + \left(m_V l K_{\dot{\varphi}}\right)s + \left(m_B + m_V\right)\left(m_V g l\right) - m_V{}^2 l^2 s^2 + m_V l K_\varphi\right] = 0 \tag{6}$$

It can be seen from this equation that the $K_{\dot{\varphi}}$ gain, in the coefficient of s, will supply damping to the system, and the K_φ gain will increase the pendulum frequency and keep the bridge above the suspended vehicle.

The bridge drive unit is an electrohydraulic unit consisting of a synchronous electric motor which drives a variable-displacement hydraulic pump. Control of the bridge is exercised by the operation of a pump stroker, which controls the displacement of this pump. The pump drives fixed-displacement hydraulic motors attached to the wheels of the bridge. A fixed displacement of the stroker produces a steady-state constant velocity of the bridge.

Since the stroker controls bridge velocity instead of bridge acceleration, the control function of accelerating the bridge as a function of pendulum angle is achieved by displacing the stroker as a function of the integral of the pendulum angle, and the function of accelerating the bridge as a function of rate of change of pendulum angle is achieved by displacing the stroker as a function of pendulum angle.

The predominant dynamic characteristic of the drive unit is the oscillatory response of bridge velocity to stroker displacement that results from the compressibility of the hydraulic fluid as it reacts against the mass of the bridge. This dynamic characteristic is expressed by the equation:

$$\frac{\dot{x}_B}{\text{Stroker displacement}} = \frac{C_1/D_m}{\frac{V}{\beta}\frac{J_L}{D_m{}^2}s^2 + \frac{J_L K_L}{D_m{}^2}s + 1} \tag{7}$$

where

C_1 oil volume delivered by pump per unit displacement of stroker, in^3/unit $\left(cm^3/\text{unit}\right)$

D_m motor displacement, 28 in^3/rad $\left(460\ cm^3/rad\right)$

β bulk modulus of oil, 1×10^5 psi $\left(6.9 \times 10^8\ N/m^2\right)$

V oil volume under compression, 600 in^3 (9850 cm^3)

J_L total inertia of load reflected at motor output shaft, 3050 in-lb-sec^2 (345 m-N-sec^2)

K_L leakage coefficient, $\frac{in^3/sec}{psi}$ $\left(\frac{cm^3/sec}{N/m^2}\right)$

For the system under study, the natural frequency of the drive unit as determined by this equation is 6.5 rad/sec. The detailed analysis of the system naturally included this characteristic. However, instead of using the transfer function presented in equation (7), a nonlinear representation for the hydraulics was used in the analysis. This representation is presented in appendix A.

Another important dynamic characteristic of the system is the oscillatory characteristic of the cable. Cable vibrations add to the measured cable angle and therefore add a spurious signal to the control signal. Equations for the first two modes of vibration for different fixed cable lengths were determined and used in the analysis. These equations included the effect of a lumped mass located near the vehicle representing the whiffletree which is a part of the vehicle suspension system. The derivation of these equations is given in appendix B. The frequency of the first mode for a 200-foot (61 m) cable length was 8.72 rad/sec which is very close to the natural frequency of the drive unit, and therefore, it put a limit on the precision with which the bridge could track the vehicle. This vibration frequency is a function of cable length and vehicle weight. The analysis was made for fixed cable lengths and vehicle weights.

Pilot Transfer Function

The pilot transfer functions, which were used in conjunction with the lunar-landing simulator equations, are derived in reference 1 and are repeated here. These transfer functions were obtained from tests made with simplified fixed-base simulators. As is pointed out in reference 1, a combination of tests were used to obtain these transfer functions. Multi-axes compensatory tracking tests using automatic parameter tracking methods to determine the response of the pilot were used to obtain the inner-loop transfer functions. Multi-loop simulations and trial-and-error methods were used to obtain the outer-loop transfer functions. It should be noted that slightly different transfer functions have been measured with different pilots and that the particular transfer function selected for this study represents a nominal pilot response.

The pilot-vehicle system involved in the landing maneuver is a multi-loop system described by the block diagram presented in figure 2. The inner loop deals with the attitude control of the vehicle. The vehicle response to attitude control was assumed to contain a proportional rate feedback and is given by the equation:

$$\frac{\theta}{\delta} = \frac{0.5}{s(s + 0.5)} \tag{8}$$

which defines a rate command system with a time constant of 2.0 seconds. Reference 1 demonstrates that a pilot's response in such an inner loop is given by:

$$\frac{\delta}{\theta_e} = \frac{K_1\tau\left(1 + \frac{K_2 s}{\tau}\right)}{(s + \tau)^2} = \frac{96(1 + 0.4s)}{(s + 6)^2} \tag{9}$$

The combination of the pilot and vehicle gives this inner loop a closed-loop characteristic frequency of 1.2 rad/sec and a damping ratio of 0.26.

The outer loop of the system deals with the longitudinal translation, and the vehicle response to attitude angle is given by a pure inertial response

$$\frac{x_V}{\theta} = \frac{5.36}{s^2} \tag{10}$$

The relation is derived from the linearized equation of motion for the horizontal component of acceleration due to the 1/6g thrust that would be in effect in the lunar environment,

$$\ddot{x}_V = \frac{1}{6} g \sin\theta \tag{11}$$

When small-angle linearization is used,

$$\ddot{x}_V = \frac{1}{6} g\theta = 5.36\theta \text{ ft/sec}^2 = 1.63\theta \text{ m/sec}^2 \tag{12}$$

$$\frac{\ddot{x}_V}{\theta} = 5.36 \frac{\text{ft/sec}^2}{\text{rad}} = 1.63 \frac{\text{m/sec}^2}{\text{rad}} \tag{13}$$

Reference 1 demonstrates that the pilot response in such an outer loop is

$$\frac{\theta_c}{x_e} = \frac{0.9(1 + 9.2s)}{(s + 10)^2} \tag{14}$$

When all these transfer functions are combined, block diagram algebra being used, a characteristic response of the complete system is obtained which has two small real roots, $s = -0.167$ and $s = -0.336$. In terms of an oscillatory response, these two roots define an overdamped response with a natural frequency given by

$$\omega_n = \sqrt{(0.167)(0.336)} = 0.236 \text{ rad/sec} \tag{15}$$

This system frequency characterizes the translation response of the system. Since the response characteristic of the longitudinal drive system of the simulator must have a response frequency higher than that of the system which is to be tested, this calculated response characteristic of the pilot-controlled translation response provides a first rough criterion for the required characteristic of the longitudinal drive system.

ANALYSIS AND TEST RESULTS

Initial Study

A detailed analytical study was made to determine the drive system characteristics and to evaluate the suitability of these characteristics for the purposes of the simulation. The complete computer program used in this study including the drive system, the cable dynamics, and the pilot-controlled vehicle is presented in figure 3. The system parameters based on the physical constraints of the simulator were estimated.

The first phase of the study was conducted to determine the response characteristics of the bridge. Open-loop step thrust inputs to the vehicle were used as the forcing function in these studies. The results showed that the presence of the cable vibration modes of motion in the system placed an upper limit on the pendulum damping gain $K_{\dot{\varphi}}$. If this gain was adjusted too high, the first vibration mode would become unstable, as is illustrated in figure 4.

The limit on the pendulum damping gain placed further restriction on the pendulum frequency gain K_{φ}. Representative system characteristics of vehicle velocity response to a 2-second thrust impulse are shown in figure 5. The oscillatory nature of these responses is the result of the bridge drive system characteristics. It can be seen that a well-damped response with a frequency of 1.57 rad/sec (a period of 4 seconds) or a poorly damped response with a frequency of 2.5 rad/sec (a period of 2.5 seconds) could be achieved.

Both of these frequencies are above the 0.236 rad/sec frequency for the pilot-controlled translation response of the lunar-landing system derived in the previous section. However, it cannot be confidently concluded that these frequencies are high enough to have no effect on the simulation. To determine the effect that the bridge response might have on the pilot-controlled maneuver, the analytical representation of the pilot and vehicle were included in a closed-loop representation of the complete system, and the response to a commanded 225-foot (69 m) displacement was determined. The results are presented in figure 6 which shows (1) the response of the pilot-vehicle combination alone, and (2) the response of the pilot-vehicle-simulator combination with the two different simulator characteristics presented before. By using the pilot-vehicle combination response as the standard for comparison, it can be seen that including the simulator bridge dynamics in the loop does indeed influence the response. With the lower gain (lower frequency) bridge control, the system is degraded to the point of instability. It was, therefore, concluded that the simulator should be operated with a frequency response as high as possible and that even then some influence of the simulator dynamics may be reflected in pilot control responses.

Post-Analysis Tests

When the lunar-landing simulator was put into operation, the system characteristics which could be achieved with the actual mechanism were determined. It was found that the highest stable pendulum frequency that could be obtained was 1.4 rad/sec (a period of 4.5 seconds). By lowering the K_{φ} gain, a well-damped response with a frequency of 0.8 rad/sec (a period of 8 seconds) could be obtained. Time histories of cable angle response to open-loop thrust impulses with these two systems are shown in figure 7. The 4.5-second and 8-second period pendulum responses are clearly seen in this figure as well as the higher frequency cable vibration modes of motion.

Runs in which a pilot closed the pitch and displacement loops were then made with both the high-gain and low-gain systems to check the results of the analytical study. These tests were started with the vehicle hovering at an altitude of approximately 30 feet (9 m). The pilot attempted to translate a prescribed distance and establish a hover over a mark located on the ground. Runs with the two systems were made one right after the other so that, insofar as possible, all environmental conditions other than the change in bridge response would be the same.

It should be noted that the vehicle attitude-control system used in the simulator was different from the representation used in the analytical study. A rate feedback was incorporated in the simulator, but the jet thrusters were operated in an on-off mode rather than in a proportional or modulated mode. The angular acceleration provided by the on-off system was $8^{o}/sec^{2}$ and the maximum angular velocity was $30^{o}/sec$. It is felt that the effects of the changes in the outer-loop bridge drive characteristics would be sufficiently well defined with each of the two attitude control systems so that the effects as obtained in the analytical study and in the simulator could be compared.

Figure 8 is the recorded time history obtained in one of the lunar-landing simulator tests. In this test the first maneuver, from the 50-foot (15 m) mark to the 275-foot (84 m) mark, was done with the high-gain system. At the 50-second point, while the pilot was turning 180^{o}, the drive system gain was adjusted to the lower setting, and the pilot started to go back toward the 50-foot (15 m) mark. The general nature of these maneuvers is very similar to that of the computed responses. With the high-gain system the pitch angle was well controlled, and with the low-gain system a decrease in the damping of the pitch-angle response can be seen at about 75 seconds. The pilot did not complete the translation in this maneuver, but landed when he stopped the pitch oscillation because of a low fuel state.

A series of tests was made at a later date than the tests presented in figure 8. Some additional refinements had been included in the bridge drive control system. Time histories of the cable-angle response to step commands in bridge acceleration for the refined bridge drive system are shown in figure 9. The periods of the bridge motion were 5 and 8 seconds with the high and low gains, respectively. The damping characteristics

of the bridge were improved. Figure 10 is a reproduction of the time histories obtained in these tests in which a 100-foot (30 m) translation was performed, and additional time was spent in holding the hover condition. In this particular test the low-gain system was tested first, and then the high-gain system. Once again the decrease in the damping of the pitch-angle response can be clearly seen.

All the pilots commented that they experienced an increase in difficulty in performing the maneuvering with the low-gain system. One pilot reported that he felt he was in "pilot-induced oscillation" condition with the low-gain system.

Iterated Analytical Study

Since the lunar-landing simulator characteristics that were achieved with the actual mechanism were not the same as those determined in the analytical study, and since the pilot's response showed a lower pitch-attitude angle limit in the flight tests than was assumed in the analytical study, the analytical study was repeated in an attempt to reproduce more closely the flight time histories. In these repeated calculations the drive system gains were adjusted to give a poorly damped, 4.5-second-period pendulum mode of motion in one case, and a well-damped, 8-second period mode in the second case to correspond to the two conditions that were tested in flight. The same linear transfer functions were used for the representation of the pilot. The pitch-attitude limit, which is the limit placed at the output of the outer-loop analog pilot, was adjusted to a 10^{o} value. This 10^{o} limit corresponds more closely with the limit used by the pilots in the flight tests than did the 40^{o} limit used in the initial analytical study. With this 10^{o} pitch-angle limit, a 225-foot (69 m) translation with a well-controlled attitude time history was obtained with the high-gain system, and this response is a better reproduction of the flight time history than was the initially calculated response. Once again a deterioration in damping, compared with that obtained with the high-gain system, was obtained with the low-gain system. These responses are presented in figure 11.

There are some limitations to the pilot transfer functions as they are known at the present time. For example, in the particular case studied in this paper, a mistake was made in the assumed pitch-angle limit in the initial analytical study. Also, it is known that different pilots will control a given system with different transfer functions. The effects of these differences between subjects has not been studied in this paper. There may be other factors which are incorrect in the pilot transfer functions as they are known at the present time. However, useful information obtained in the example presented in this paper does add confidence to these functions.

The general agreement between the analytical cases and the simulator cases as shown in figures 6, 8, 10, and 11 indicates that the human transfer functions are a reasonable representation of human response within limitations. It is felt that these transfer

functions are well enough defined to be employed advantageously in the design phases of similar manually controlled systems provided the limitations are recognized and are not exceeded.

Single-Loop Task

The analytical method, which was used to predict the effect of inserting a servo or servomechanism in the outer loop of a multi-loop problem in the previous sections of this paper, can also be used in single-loop or inner-loop control tasks. The primary differences in the two problems are that single-loop control tasks are operated by human controllers at much higher frequencies, and that the response of the inserted servo must, correspondingly, be much higher in order to have no effect on the system.

The analytically predicted effect of inserting first-order and second-order mechanisms in a single-axis control task are presented in figure 12(a). The vehicle dynamics considered here is a pure acceleration $\frac{\theta}{\delta} = \frac{2}{s^2}$. The transfer function used to represent the pilot was taken from reference 1 and is

$$\frac{\delta}{\theta_e} = \frac{56(1 + 1.35s)}{(s + 7)^2} \tag{16}$$

The closed-loop response of this system contains an oscillatory characteristic with an undamped natural frequency of 3.3 rad/sec and a damping ratio of 0.36.

The effect on the closed-loop characteristics of this system that results from adding a first-order lag to the dynamics of the form $\frac{\tau_f}{s + \tau_f}$ is also shown in figure 12(a). The value of the breakpoint frequency τ_f was varied from 100 down to zero, and the change in system closed-loop damping ratio and natural frequency is plotted. Very drastic changes occur in the system response if the breakpoint frequency is reduced below 20 rad/sec.

The effect of adding a second-order servo to the dynamics is also shown. The form of this inserted mechanism is $\frac{\omega_{n,f}^2}{s^2 + 2(0.7)\omega_{n,f}s + \omega_{n,f}^2}$. The assumed natural frequency ω_n was varied from 50 to 0, and the damping ratio was held constant at 0.7. The effect of inserting such a mechanism in the control loop is similar to that of the first-order lag, but more severe. Again, very drastic changes occur if the natural frequency is dropped below 20 rad/sec.

Reference 3 presents results of an experimental study that is very similar to the single-loop analysis. In this experimental study the vehicle dynamics were representative of an aircraft longitudinal control system. A fixed-base simulation of a

landing-approach task was used for the control problem. A second-order representation of the elevator actuator was inserted in the control loop. The natural frequency of the actuator was varied from 62 rad/sec (10 cycles per second) down to 6.2 rad/sec (1 cycle per second). Pilot ratings were obtained for a number of natural frequencies within the range and are shown in figure 12(b). The damping of the second-order response was held constant at a damping ratio of 0.7. Very drastic changes in pilot ratings were obtained as the natural frequency was reduced below the 18 to 30 rad/sec range. Typical ratings were 2.5 (good, acceptable) for natural frequencies of 18 rad/sec and above, and 6 (unsatisfactory) at a natural frequency of 6 rad/sec. From these results it can be seen that the experimental study confirms the analytical study of the single-loop, or inner-loop, problem.

CONCLUDING REMARKS

The results of this study have indicated that the human transfer functions, subject to the conditions of this experiment, are a reasonable representation of human response. These transfer functions appear to be defined well enough to be used to establish system specifications in the design phases of systems similar to those in the two examples presented in this paper. However, experience with these transfer functions is still very limited, and care should be taken in extending their use to other particular applications.

The results of the two examples studied show that the frequency response of the control system elements should be kept as high as possible to minimize the lag between the pilot's inputs and the system outputs. In the case of the lunar-landing simulator, it is concluded that the maneuvers performed with the simulator will involve dynamics which are possibly more difficult to control than the dynamics of the lunar module in the lunar environment.

Langley Research Center,
National Aeronautics and Space Administration,
Langley Station, Hampton, Va., July 7, 1969.

APPENDIX A

BRIDGE EQUATIONS

The dynamic response of the hydraulic system was represented by the following equations:

$$Q_p = \omega_p D_p \tag{A1}$$

$$Q_m = \omega_m D_m \tag{A2}$$

$$Q_L = \pm K_o A_L \left|\sqrt{p_m}\right| \tag{A3}$$

$$Q_{RL} = \pm K_o A_{RV} \left|\sqrt{p_m}\right| \tag{A4}$$

where ω_p is determined by the dynamic equation

$$T_m = K_m\left(\omega_{sync} - \omega_p\right)$$

Thus

$$Q_c = Q_p - Q_m - Q_L - Q_{RL} \tag{A5}$$

and also

$$Q_c = \frac{V}{\beta}\dot{p}_m \tag{A6}$$

The relationships between hydraulic pressure and bridge velocity are then

$$J_m\dot{\omega}_m = p_m D_m - B_m\omega_m - \frac{T_L}{n} \tag{A7}$$

$$T_L = K_t\left(\psi_m - \psi_L\right) \tag{A8}$$

$$J_L\frac{\ddot{x}_B}{R} = T_L - B_L\frac{\dot{x}_B}{R} \tag{A9}$$

Other nonlinear or dynamic factors included in the representation were (1) the time constant and limit displacement of the stroker and (2) selection of the gearing.

APPENDIX B

CABLE MODES OF VIBRATION

Sketch (b) shows the assumed representation for the cable, and the terms used in the derivation of the cable equations of motion:

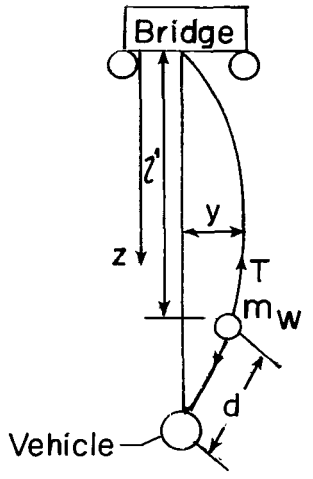

Sketch (b).- Cable and whiffletree.

Assume that a solution exists in the form

$$y = h \sin kat \sin kz \tag{B1}$$

where

$$a^2 = \frac{T}{w'/g}$$

T tension

w' weight per foot (per meter) of cable

A boundary equation, for the motion of the whiffletree, which must be satisfied is

$$m_w\left(\frac{d^2y}{dt^2}\right)_{z=\ell'} = -T\left(\frac{dy}{dz}\right)_{z=\ell'} + \frac{Ty_{z=\ell'}}{d} \tag{B2}$$

Manipulation of equations (B1) and (B2) gives

$$\left(-m_w k^2 a^2 + \frac{T}{d}\right)\tan k\ell' = -Tk \tag{B3}$$

APPENDIX B

An iterative procedure was used to solve equation (B2) for k, where

$$m_w = 6.2 \text{ slugs } (89 \text{ kg})$$

$$w' = 0.8 \text{ lb/ft } (1.2 \text{ kg/m})$$

$$T = \frac{5}{6} m_V = 8340 \text{ lb } (3700 \text{ N})$$

$$\ell' = 200 \text{ feet } (61 \text{ m})$$

$$d = 6 \text{ feet } (1.83 \text{ m})$$

The value of k for the first mode of vibration was 0.015, and the frequency $\omega_n = ka = 8.72$ rad/sec. The Lagrange equation was then used to determine the coupling between the bridge motion, the pendulum motion, and the cable vibration. For the first mode of vibration, the equation for the motion of the cable and whiffletree is

$$y = h \sin 8.72t \sin 0.015z$$

and the velocity can be written

$$\dot{y} = \dot{h} \sin 0.015z$$

the kinetic energy of the cable is, therefore,

$$\text{Kinetic energy} = \frac{1}{2} \frac{w'}{g} \int_0^{200} \left(\dot{h} \sin 0.015z + \dot{x} + z\dot{\theta}\right)^2 dz$$

$$= 1.29\dot{h}^2 + 3.28\dot{x}\dot{h} + 344\dot{\theta}\dot{h} + 2.48\dot{x}^2 + 496\dot{x}\dot{\theta} + 33\,200\dot{\theta}^2$$

the kinetic energy of the whiffletree, located at z = 200, is

$$\text{Kinetic energy} = \frac{1}{2} m_w \left\{\left[\dot{h} \sin 0.015(200)\right] + \dot{x}^2 + 200\dot{\theta}\right\}^2$$

$$= 0.06\dot{h}^2 + 3.1\dot{x}^2 + 12\,4000\dot{\theta}^2 + 0.86\dot{h}\dot{x} + 172\dot{h}\dot{\theta} + 1240\dot{x}\dot{\theta}$$

By applying the Lagrange equation, additional terms for the x and θ equations, and the h equation were then determined

$$\left(m_V + m_B + 11.2\right)\ddot{x}_B + \left(m_V\ell + 1736\right)\ddot{\theta} + 4.14\ddot{h} = K_\varphi \varphi + K_{\dot{\varphi}}\dot{\varphi} \qquad \text{(B4)}$$

APPENDIX B

$$\left(m_V l + 1736\right)\ddot{x}_B + \left(m_V l^2 + 314\ 400\right)\ddot{\theta} + m_V g l\theta + 516h = 0 \tag{B5}$$

$$2.70\ddot{h} + 4.14\ddot{x} + 516\ddot{\theta} + 206h = 0 \tag{B6}$$

where, according to Rayleigh's principle, the coefficient of h in the h equation (eq. (B6)) has been set so that the uncoupled frequency of the first mode of vibration will be the same as that determined previously, 8.72 radians per second.

REFERENCES

1. Adams, James J.; Bergeron, Hugh P.; and Hurt, George J., Jr.: Human Transfer Functions in Multi-Axis and Multi-Loop Control Systems. NASA TN D-3305, 1966.

2. O'Bryan, Thomas C.; and Hewes, Donald E.: Operational Features of the Langley Lunar Landing Research Facility. NASA TN D-3828, 1967.

3. Parrag, Michael L.: Pilot Evaluations in a Ground Simulator of the Effects of Elevator Control System Dynamics in Fighter Aircraft. AFFDL-TR-67-19, U.S. Air Force, Sept. 1967.

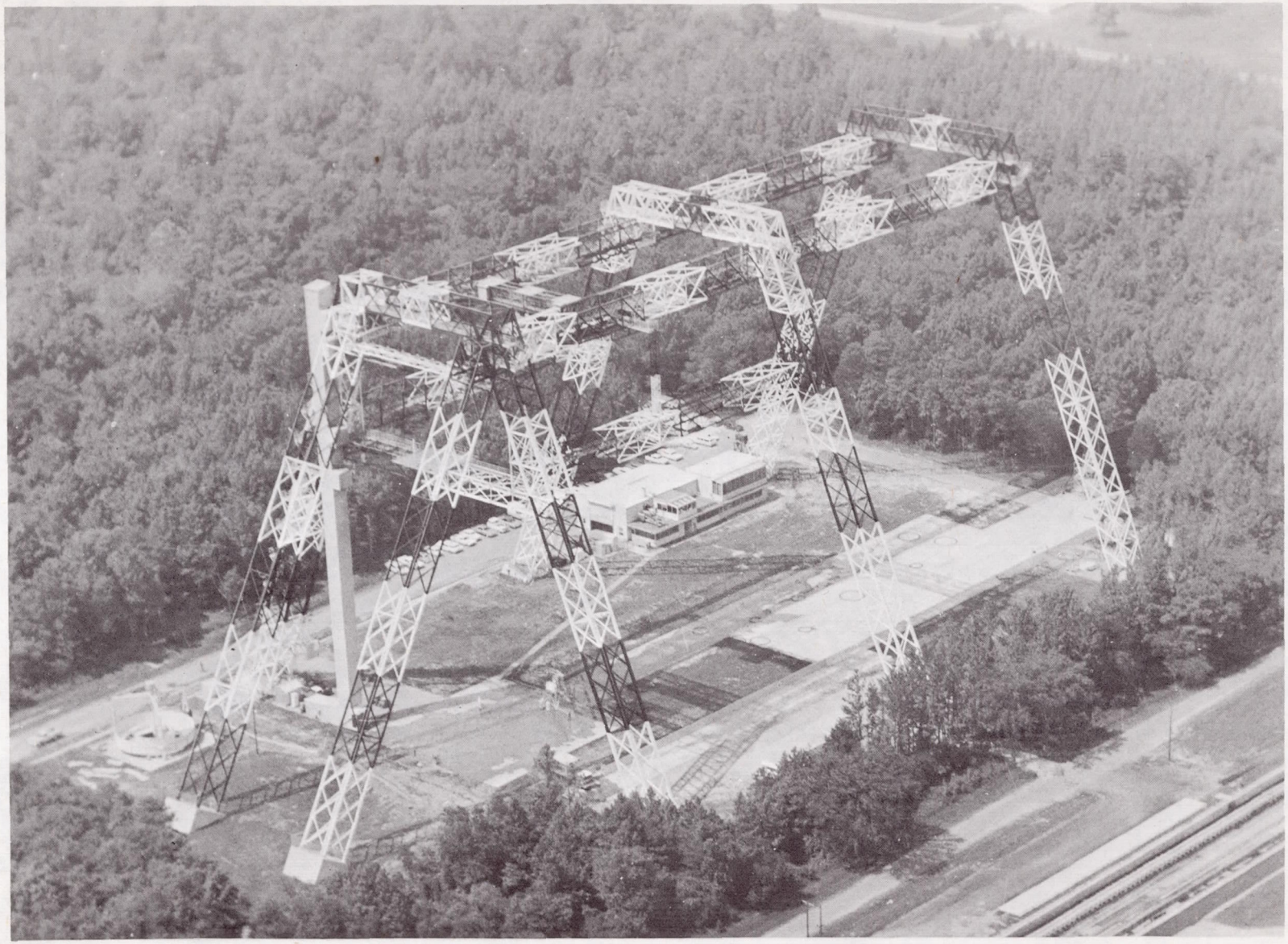

Figure 1.- Lunar-landing simulator.

L-68-6959

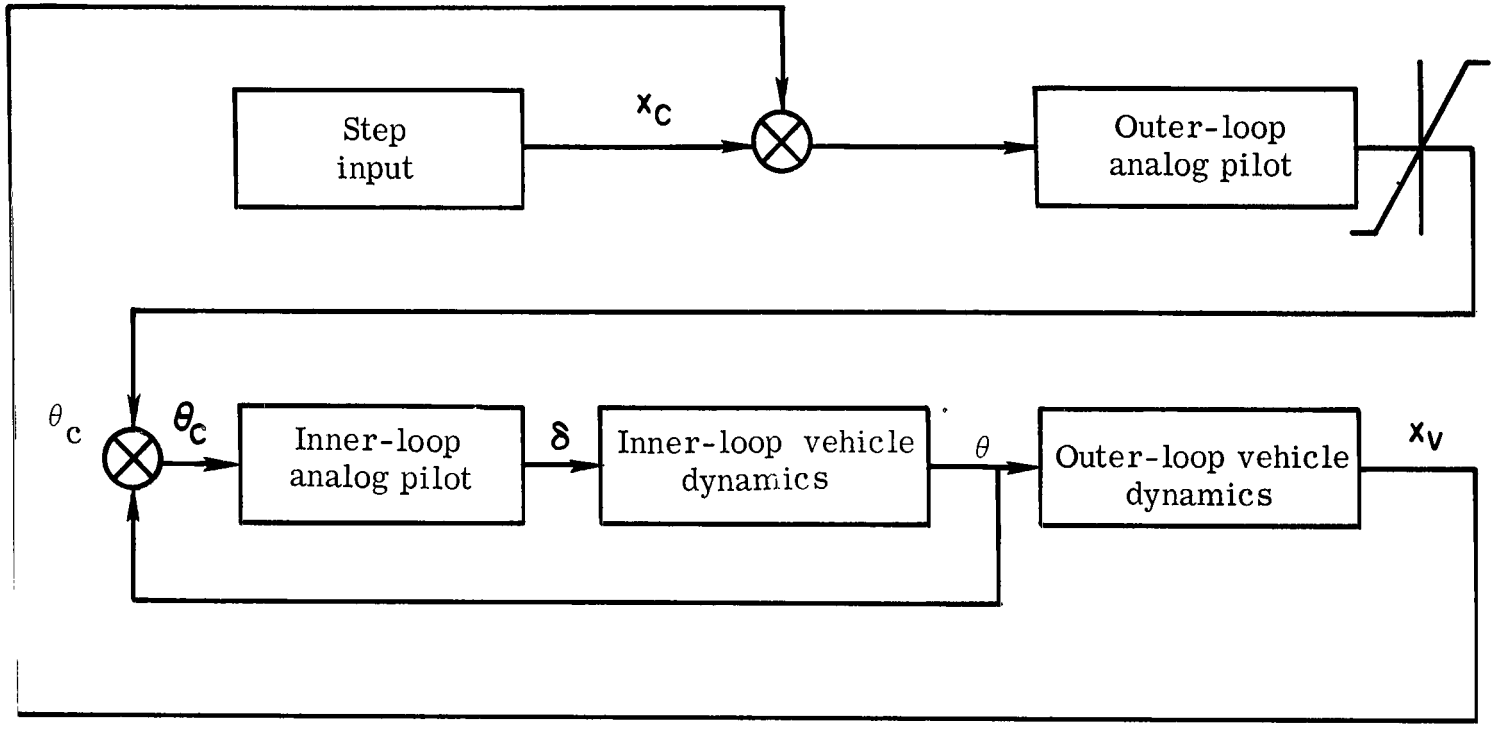

Figure 2.- Block diagram of the double control loop.

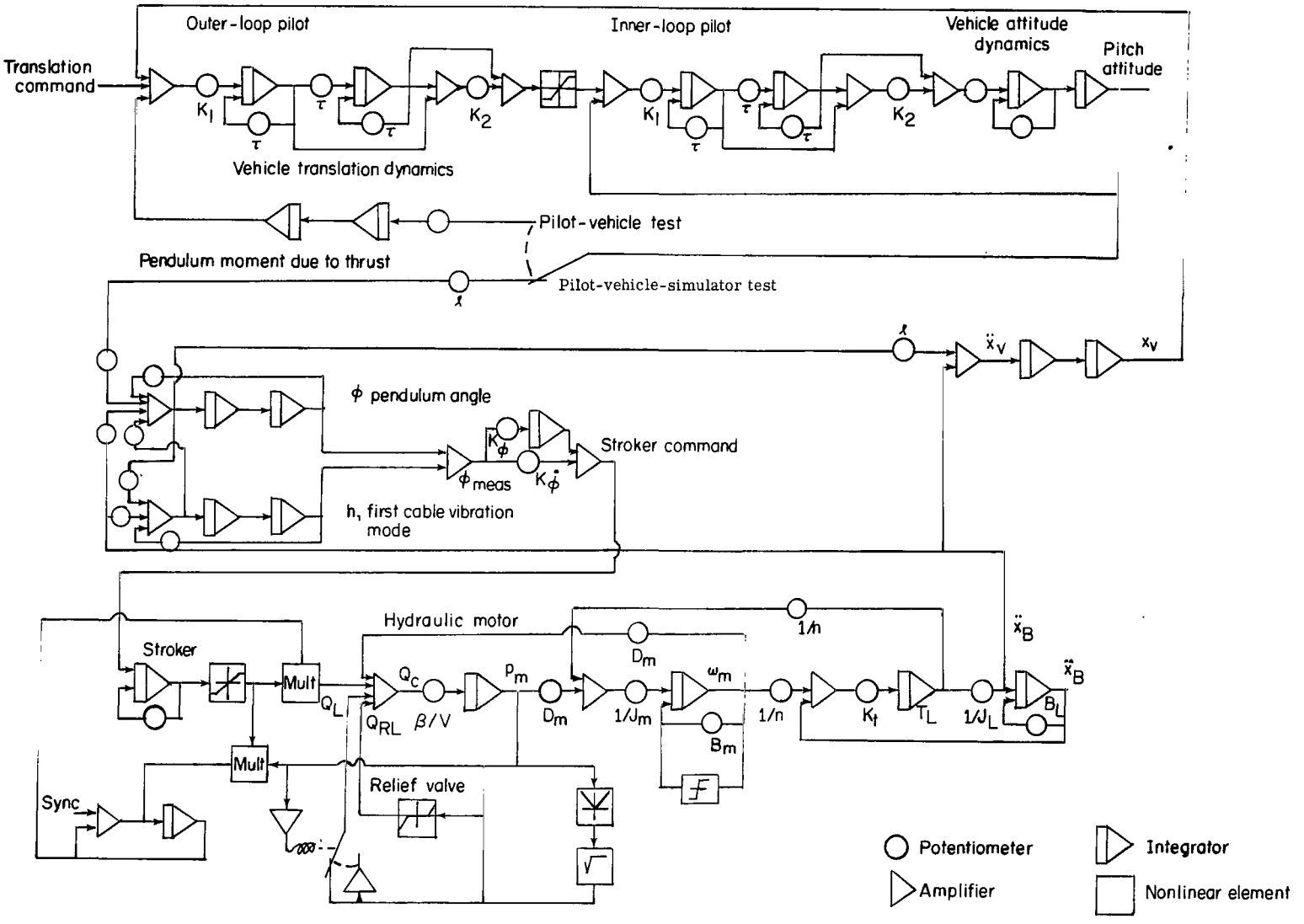

Figure 3.- Diagram of pilot-vehicle-simulator system.

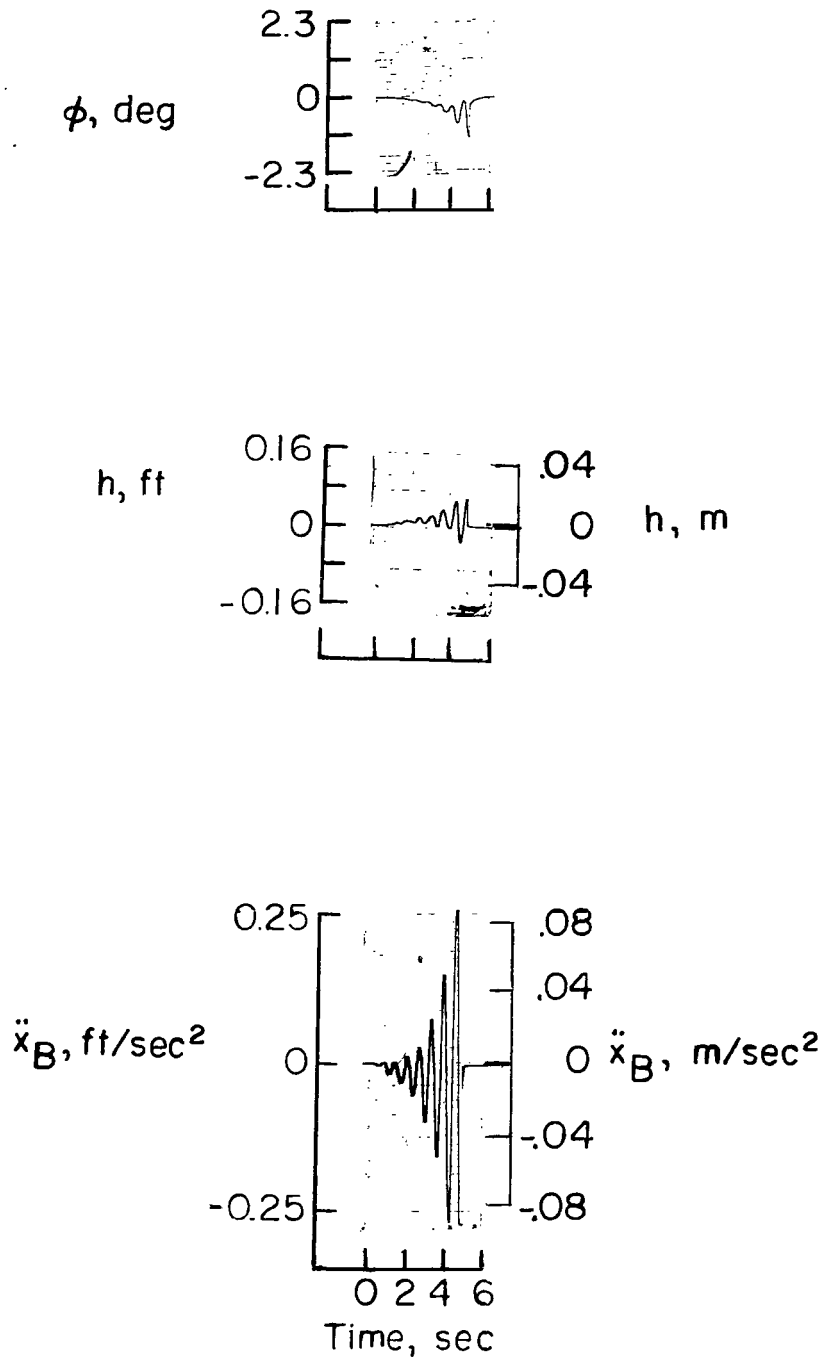

Figure 4.- Calculated cable divergence.

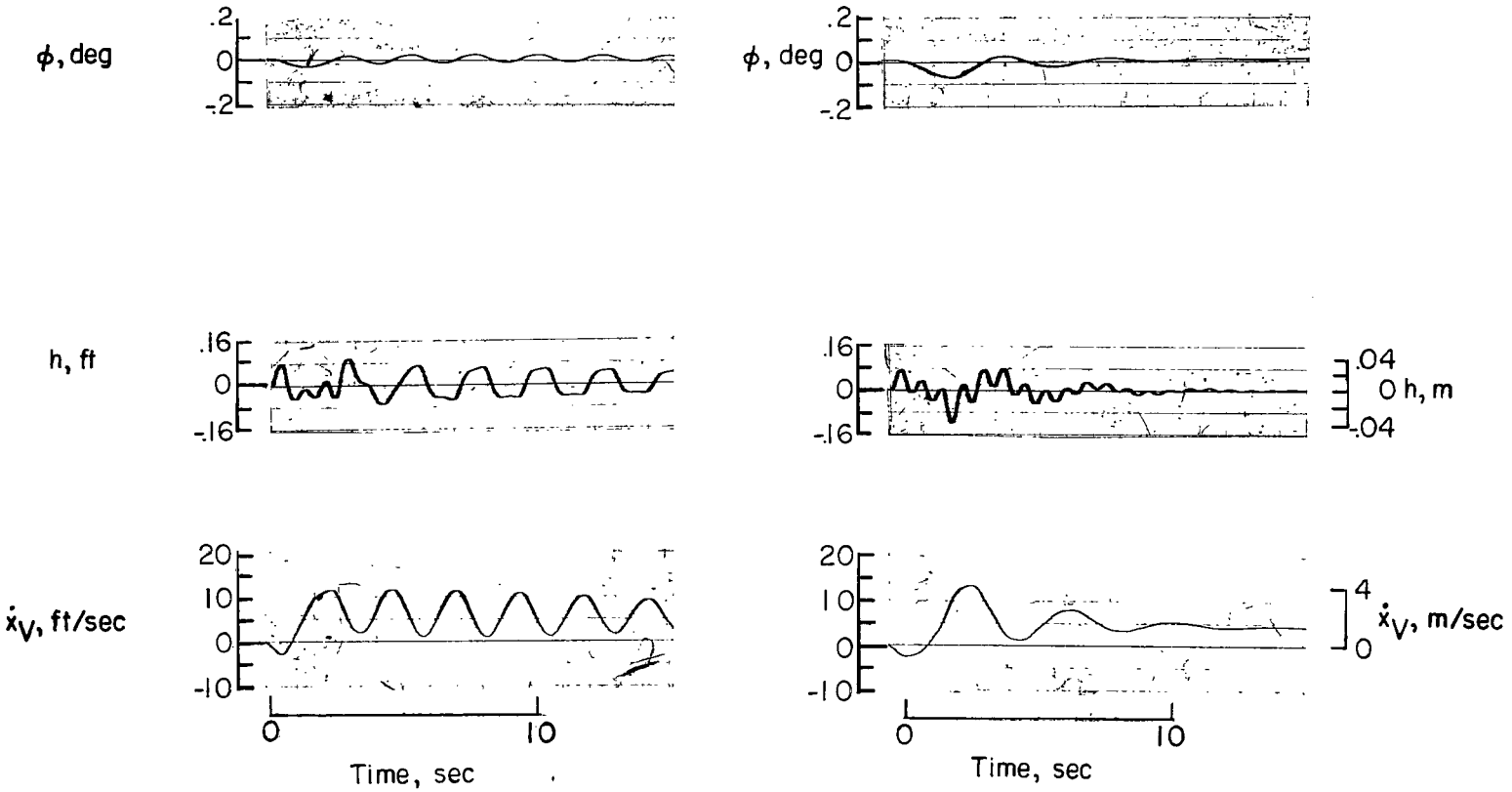

(a) High gain.

(b) Low gain.

Figure 5.- Calculated response of simulator to a 2-second thrust impulse.

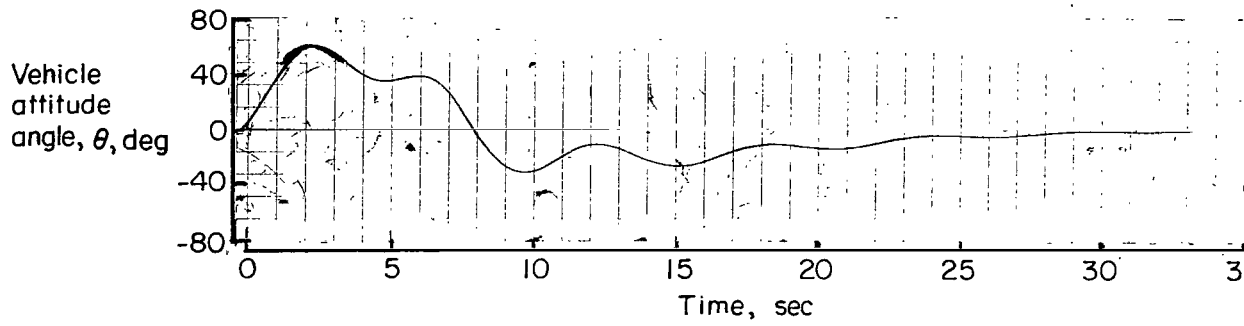

(a) Pilot-vehicle combination.

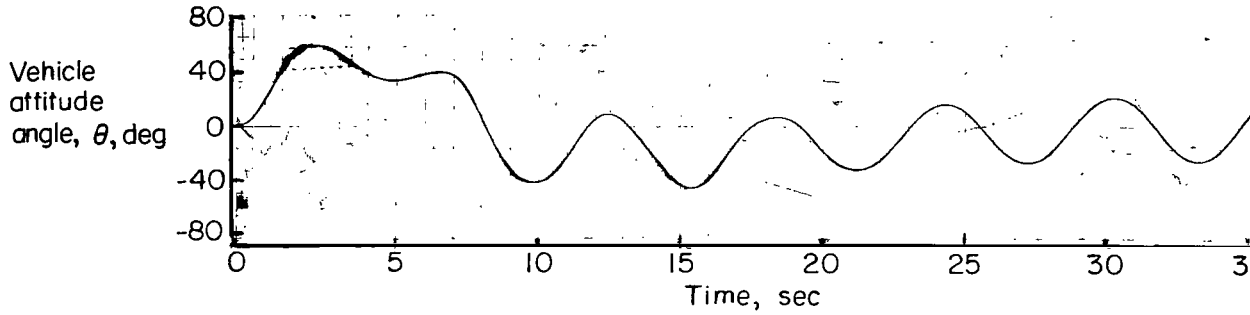

(b) Pilot-vehicle-simulator combination with high gain simulator.

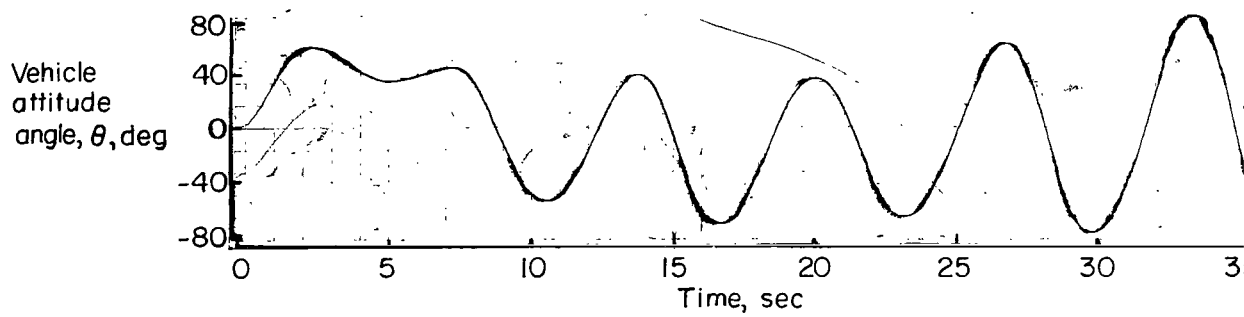

(c) Pilot-vehicle-simulator combination with low gain simulator.

Figure 6.- Calculated vehicle attitude response to a 225-foot (69 m) step translation command.

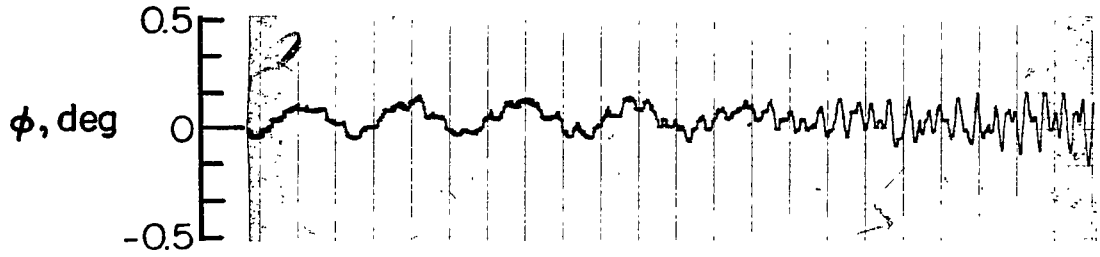

(a) High gain.

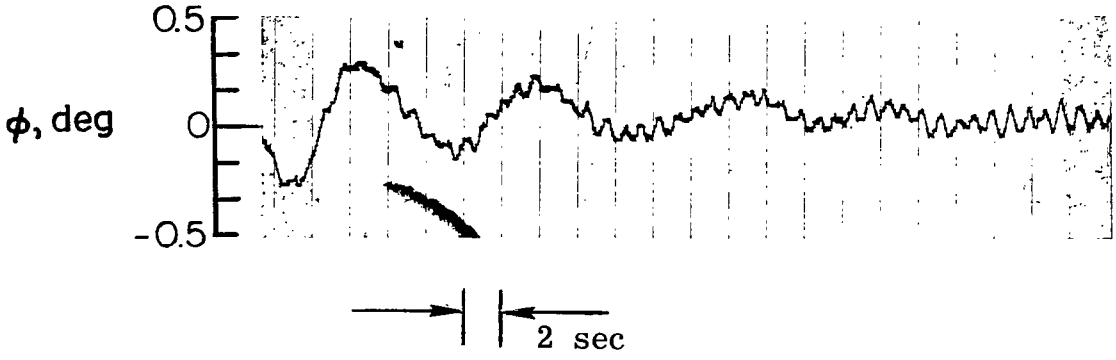

(b) Low gain.

Figure 7.- Lunar-landing simulator cable-angle response to small inputs.

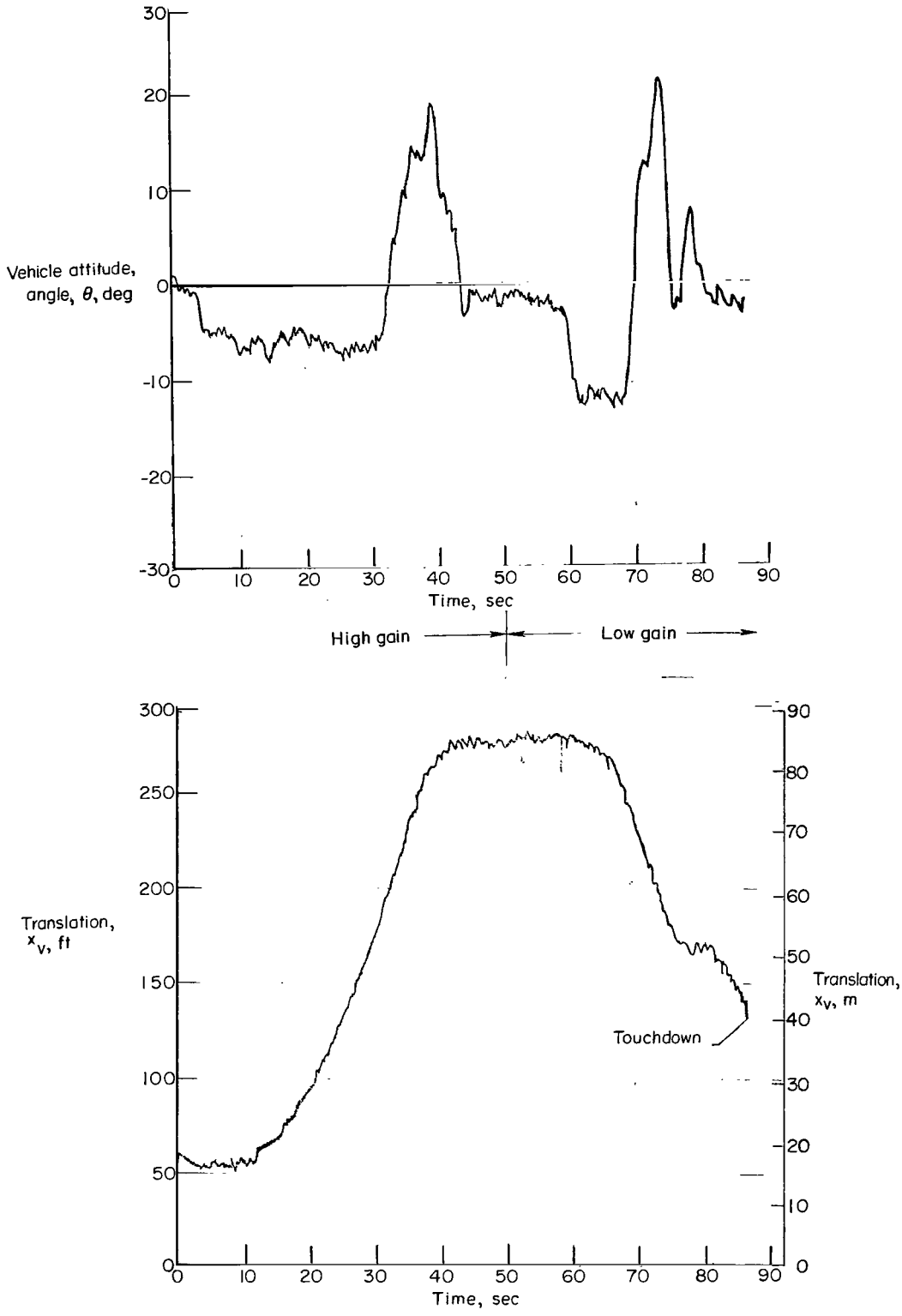

Figure 8.- Lunar-landing simulator response to a 225-foot (69 m) translation command with both high gain and low gain simulator control.

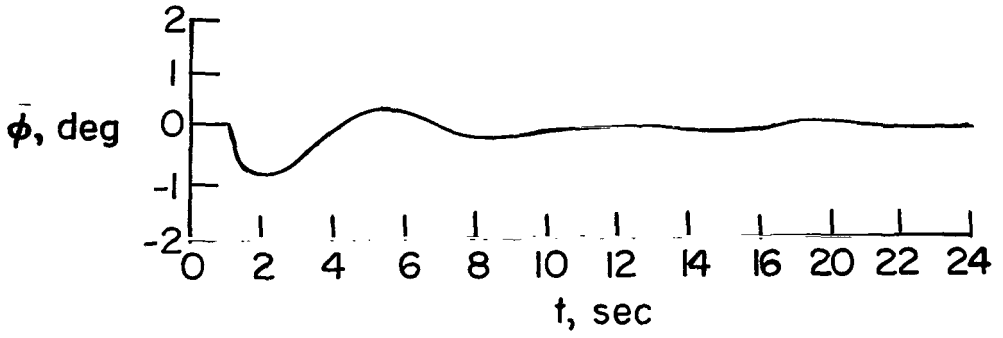

(a) High gain.

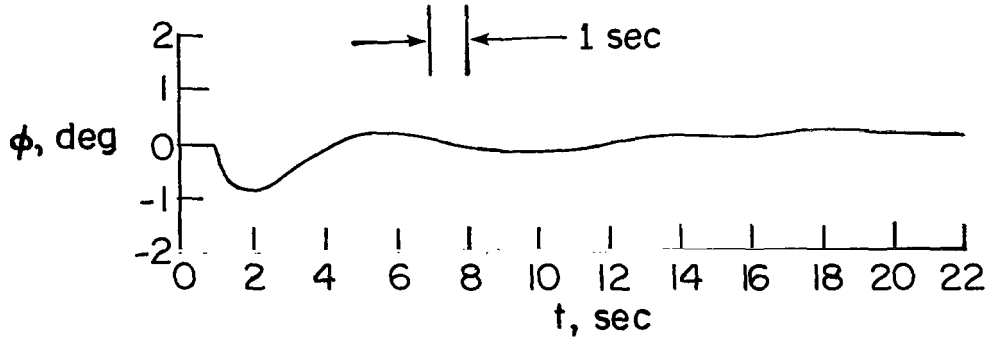

(b) Low gain.

Figure 9.- Lunar-landing simulator cable-angle response to small inputs.

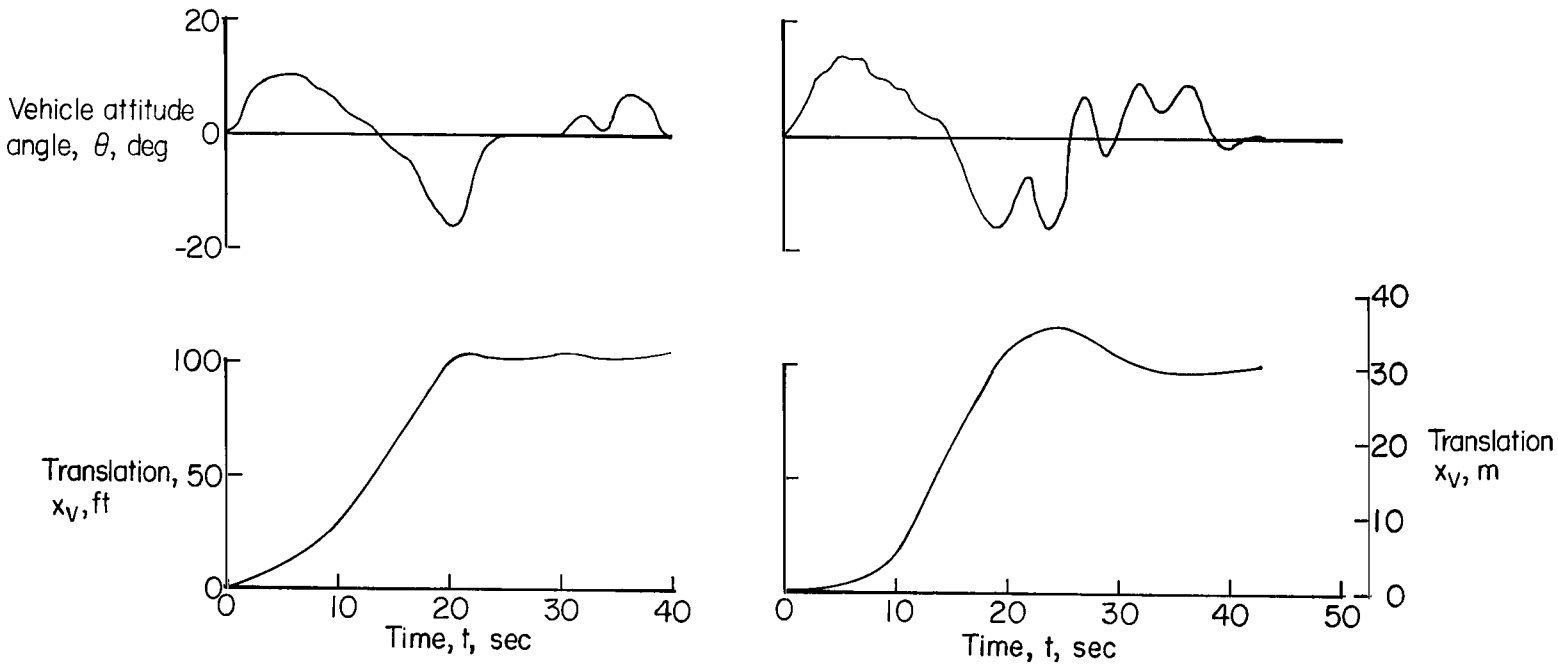

(a) High gain.

(b) Low gain.

Figure 10.- Simulator response to a 100-foot (30 m) translation command.

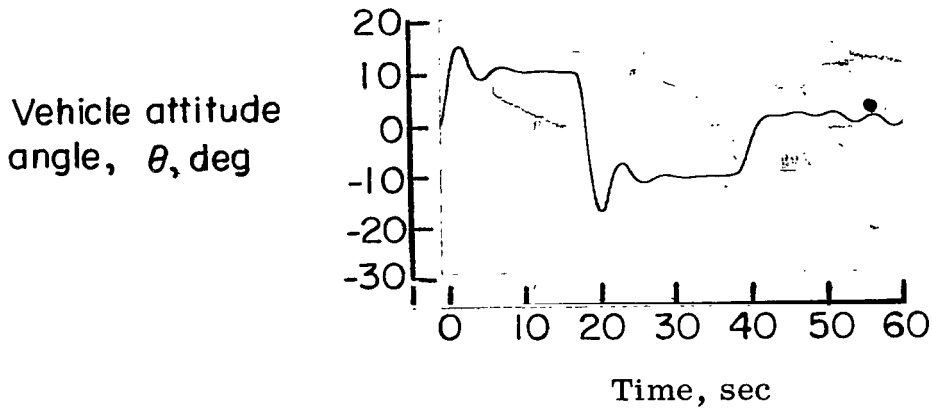

(a) Pilot-vehicle-simulator combination with low gain (4-second period) simulator.

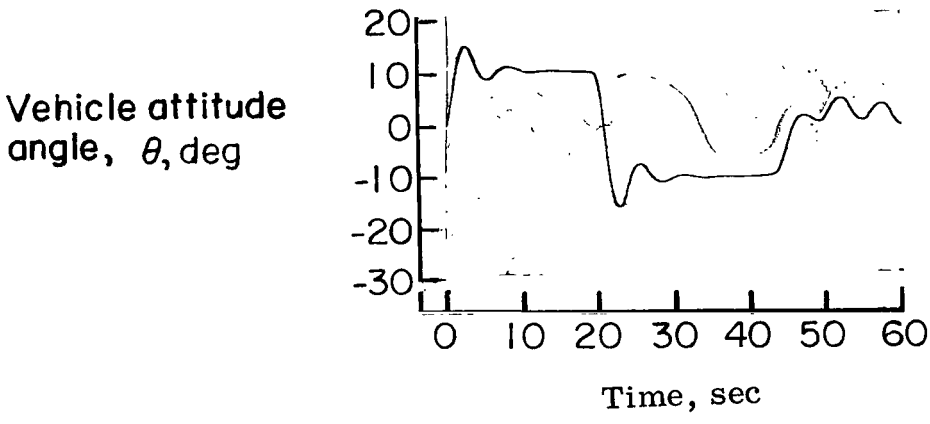

(b) Pilot-vehicle-simulator combination with very low gain (8-second period) simulator.

Figure 11.- Repeated calculation of vehicle attitude response to a 225-foot (69 m) step translation command.

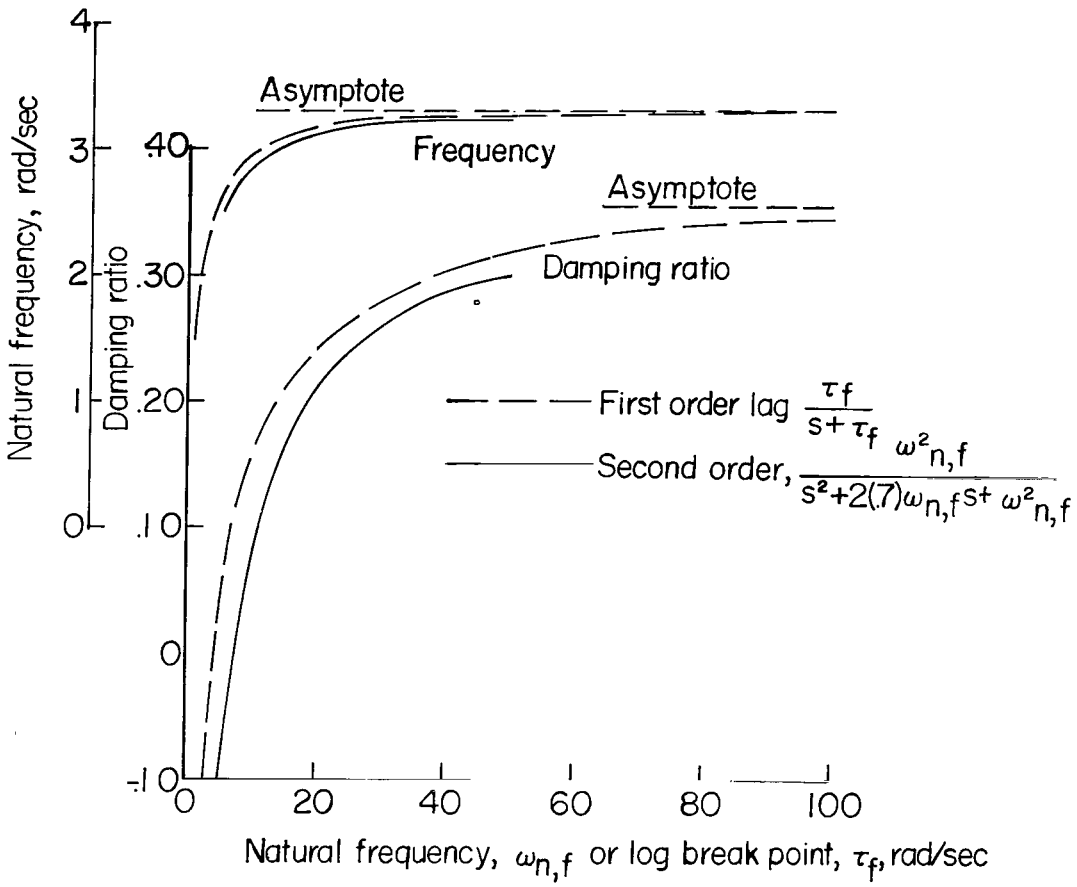

(a) Calculated system natural frequency and damping ratio as a function of τ_f or $\omega_{n,f}$.

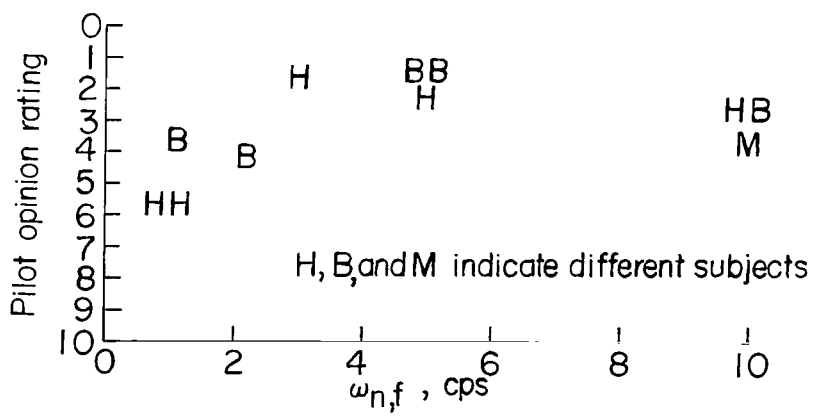

(b) Pilot opinion rating as a function of $\omega_{n,f}$ (from ref. 3, p. 57).

Figure 12.- Effect on closed loop frequency and damping ratio of inserting first- and second-order servos in a single loop control task.

NASA-Langley, 1969 — 5 L-6382